

Intriguing Property of GAN for Remote Sensing Image Generation

Xingzhe Su · Lingyu Si · Wenwen Qiang · Junzhi Yu · Fengge Wu ·
Changwen Zheng · Fuchun Sun

the date of receipt and acceptance should be inserted later

Abstract Generative adversarial networks (GANs) have achieved remarkable progress in the natural image field. However, when applying GANs in the remote sensing (RS) image generation task, we discover an extraordinary phenomenon: the GAN model is more sensitive to the size of training data for RS image generation than for natural image generation (Fig.2). In other words, the generation quality of RS images will change significantly with the number of training categories or samples per category. In this paper, we first analyze this phenomenon from two kinds of toy experiments and conclude that the amount of feature information contained in the GAN model decreases with reduced training data (Fig.3). Based on this discovery, we propose two innovative adjustment schemes, namely Uniformity Regularization (UR) and Entropy Regularization (ER), to increase the information learned by the GAN model at the distributional and sample levels, respectively. We theoretically and empirically demonstrate the effectiveness and versatility of our methods. Extensive experiments on the NWPU-RESISC45 and PatternNet datasets show that our methods outperform the well-established models on RS image generation tasks.

Keywords image generation · Generative Adversarial Networks · remote sensing

1 Introduction

The image generation task [Xu and Jordan \(1996\)](#); [Hinton and Salakhutdinov \(2006\)](#); [Ranzato et al. \(2010\)](#) aims to learn the real distribution of images, builds effective generation models, and produces various realistic images by changing some potential parameters.

Address(es) of author(s) should be given

Generative adversarial networks (GANs) [Goodfellow et al. \(2014\)](#) have made significant progress as an efficient solution to this task, especially in synthesizing high-fidelity images. Nowadays, the GAN models have become the cornerstone techniques for numerous vision applications, such as image super-resolution [Ledig et al. \(2017\)](#); [Bell-Kligler et al. \(2019\)](#); [He et al. \(2022\)](#), image inpainting [Zeng et al. \(2021\)](#); [Yu et al. \(2018\)](#), domain adaptation [Liu and Tuzel \(2016\)](#); [Choi et al. \(2019\)](#), and image-to-image translation [Park et al. \(2019\)](#); [Wang et al. \(2021\)](#).

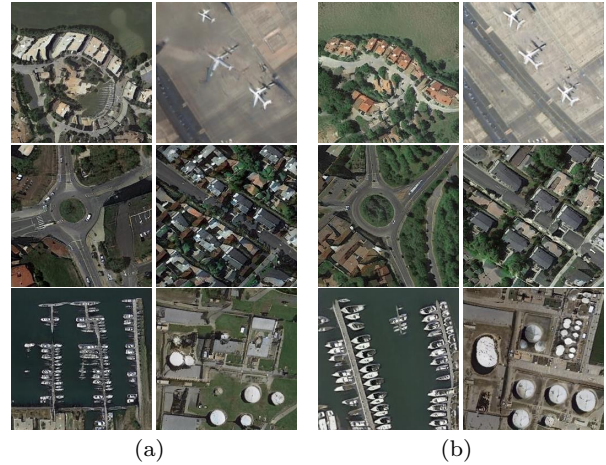


Fig. 1 (a) Remote sensing images generated by StyleGAN2+ADA. (b) Remote sensing images generated by our method. Our images have richer content and are closer to the real images.

GAN is also a favored method for the generation task in the remote sensing (RS) field. The applications of GANs in RS include augmenting training samples in classification [Lin et al. \(2017\)](#); [Yu et al. \(2019\)](#); [Wei](#)

et al. (2020), change detection Chen et al. (2021), and dealing with image-generation-related tasks such as image translation Bejiga et al. (2020); Rui et al. (2021); Chen et al. (2020); Zhao et al. (2021) and image super-resolution Jiang et al. (2019); Xiong et al. (2020). However, the RS images synthesized by these methods are of low quality. To tackle this issue, an alternative is to directly apply the well-established GAN models to RS image generation tasks. During the experiments, we found an unusual phenomenon that has not been seen in natural image generation tasks, that is, the generation quality of remote sensing images will change significantly with different sizes of training data.

To be more specific, we perform image generation experiments on the NWPU-RESISC45 dataset Gong et al. (2017) in the same settings as previous work Shahbazi et al. (2022). We gradually reduce the training data size by reducing the number of classes or the number of samples per class. In both cases, the Frchet Inception Distance score (FID) Heusel et al. (2017) and the Kernel Inception Distance score (KID) Bińkowski et al. (2018) gradually increase, indicating worse generation quality. The overall experiment results in Fig.2 are consistent with those of natural images. However, we find a unique phenomenon: the GAN model is more sensitive to the size of training data for RS image generation than for natural image generation. The metric scores vary more significantly than those of natural images under different numbers of training classes or samples per class. To find the reasons behind this, we analyze the features of these generated samples (Fig.3). We observe that the features get sparser as the number of training classes decreases, and the distributions of generated samples in the feature space get uneven when reducing training samples per class. Inspired by the information theory, sparser features contain less information, and the uniform distribution gets the maximum information entropy. Therefore, for the sensitivity of the GAN model to the training data size, a plausible explanation is that the amount of the feature information contained in the GAN model dramatically decreases when training data sizes are reduced, leading to poor generation quality. Consequently, this guides us to improve the generation quality of RS images by enriching the amount of feature information contained in the GAN model during training.

In this paper, we propose distribution-wise and sample-wise adjustment schemes to increase the information entropy so as to enrich the amount of feature information contained in the GAN model during training. Specifically, based on our discovery (Fig.3), we impose a uniformity regularization on the distribution of features of generated samples and an entropy regularization on

the features of the individual sample. We empirically show that these two regularization terms are effective in remote sensing image generation tasks. In summary, the contributions of this paper are the following:

- We explore the properties of GAN models on RS image generation tasks and find that the GAN model is more sensitive to the size of training data for RS image generation than for natural image generation.
- After analysis from two toy experiments, we conclude that the amount of feature information contained in the GAN model decreases dramatically with reduced training dataset.
- We propose distribution-wise and sample-wise regularization schemes, which can be applied to arbitrary GAN models, to increase the feature information learned by the models.
- Extensive experiments on various GAN approaches and datasets demonstrate the effectiveness and versatility of our methods.

2 Related Work

Generative adversarial networks. Based on the idea of the zero-sum game, GANs aim to model the target distribution using adversarial learning. Various modifications have been proposed to stabilize the training process and improve the quality of the generated samples, including training objectives Arjovsky et al. (2017); Gulrajani et al. (2017); Mao et al. (2017); Miyato et al. (2018); Mescheder et al. (2018); Jolicoeur-Martineau (2018) and network architectures Zhang et al. (2019); Brock et al. (2018); Karras et al. (2019, 2020b); Esser et al. (2021); Jiang et al. (2021b). Among these methods, BigGAN Brock et al. (2018) and StyleGAN2 Karras et al. (2020b) stand out because of the high-quality synthetic samples and the broad applications. Besides, several studies Gulrajani et al. (2018); Webster et al. (2019) raise the concern of insufficient data for training the GAN models. Recent research exploits data augmentation Zhao et al. (2020); Karras et al. (2020a); Jiang et al. (2021a) methods to increase data diversity. Besides, Liu et al. Liu et al. (2020) proposed a lighter network architecture and a self-supervised discriminator. Tseng et al. proposed the LeCam Tseng et al. (2021) regularization to prevent the discriminator from over-fitting on small data. Coupled with these methods, the performance of GAN models becomes more outstanding. However, current GAN models can generate high-resolution natural images but not realistic remote sensing images (Fig.1(a)).

GAN in the RS field. GANs have been applied to various kinds of RS images, such as infrared im-

ages Li et al. (2019), hyperspectral images Xu et al. (2018b); Abady et al. (2020) and synthetic aperture radar (SAR) images Gao et al. (2019). In this paper, we focus on RS RGB images. Existing GAN models in the RS field can be divided into two types according to their applications. This first kind is augmenting training samples Lin et al. (2017); Yu et al. (2019); Wei et al. (2020); Chen et al. (2021). Lin et al. propose MARTAGAN Lin et al. (2017), which is the first time that GANs have been applied to RS images. Chen et al. propose IAUG Chen et al. (2021), which leverages the GAN model to generate RS images that contain changes involving plenty and diverse buildings. The second kind deals with image-generation-related tasks such as image translation Bejiga et al. (2020); Rui et al. (2021); Chen et al. (2020); Zhao et al. (2021) and image super-resolution Jiang et al. (2019); Xiong et al. (2020). However, these methods do not delve into the characteristics of RS images, and the generated images are of low quality. Su et al. propose GSGAN Su et al. (2022) to generate controllable and realistic RS images. This is the first work that focuses on RS image generation tasks. However, its improvements mostly rely on intuition and lack theoretical support.

In this paper, we explore the properties of GAN models on RS image generation tasks and discover an overlooked phenomenon: the GAN model is more sensitive to the size of training data for RS image generation than for natural image generation. We further analyze this discovery in Section 3. Based on our discovery, we propose two innovative adjustment schemes, which will be explained in detail in Section 4. We empirically prove our methods are effective, versatile, and require neither modification of the network structure nor excessive computational effort (Section 5).

3 Preliminary Study and Analysis

In this section, we first introduce the basic framework of GAN. Then we explore the properties of GAN models on RS image generation tasks and find an unusual phenomenon that has not been observed on natural images. Finally, we analyze this phenomenon and propose plausible explanations.

3.1 Preliminary GANs

Based on the idea of the zero-sum game, a GAN model consists of a generator G and a discriminator D . The generator aims to generate realistic samples to fool the discriminator, while the discriminator tries to distinguish between real and fake samples. When the model

reaches the final equilibrium point, the generator will model the target distribution and produce counterfeit samples, which the discriminator will fail to discern. Let V_D and L_G denote the training objectives of the discriminator D and the generator G , respectively. The training of the GAN frameworks can be generally illustrated as follows:

$$\max_D V_D = \mathbb{E}_{x \sim P_{data}} [D(x)] - \mathbb{E}_{z \sim p_z} [D(G(z))] \quad (1)$$

$$\max_G L_G = \mathbb{E}_{z \sim p_z} [D(G(z))] \quad (2)$$

where the input vector z of G is usually sampled from the *normal distribution*.

3.2 Motivating Example

As we mentioned above, we apply the well-established GAN models to RS image generation tasks. We test the performance of GANs in the same settings as previous work Shahbazi et al. (2022). We base our experiments on StyleGAN2 Karras et al. (2020b) with adaptive data augmentation (ADA) Karras et al. (2020a). The model is trained on the NWPU-RESISC45 dataset Gong et al. (2017) (more details in Section 5.1). We perform the experiments by gradually reducing the size of the training set in two ways. In Fig.2(a), we reduce the number of classes while having 700 training images in each class. In Fig.2(b), we reduce the number of images per class while using 45 classes in all cases. In both cases, the FID and KID gradually increase, indicating worse generation quality. This observation is in line with previous work Shahbazi et al. (2022). In addition, we found an extraordinary phenomenon: the metric scores of generated RS images vary more significantly than those of natural images under different numbers of training categories or samples per category. In Fig.2(a), the fluctuations of metric scores of RS images are more significant than those of natural images (the red curve). Nevertheless, this may be related to the training data size, as there are 700 RS images per category in our experiments, compared to only 100 natural images per category in Shahbazi et al. (2022). But Fig.2(b) proves that the training data size is not the underlying cause. In Fig.2(b), we set the number of classes at 45, while the natural images have 50 classes. The fluctuations in the RS images are still more dramatic than in the natural images when the samples are reduced. It appears that the GAN model is more sensitive to the size of training data for RS image generation tasks than for natural image generation tasks.

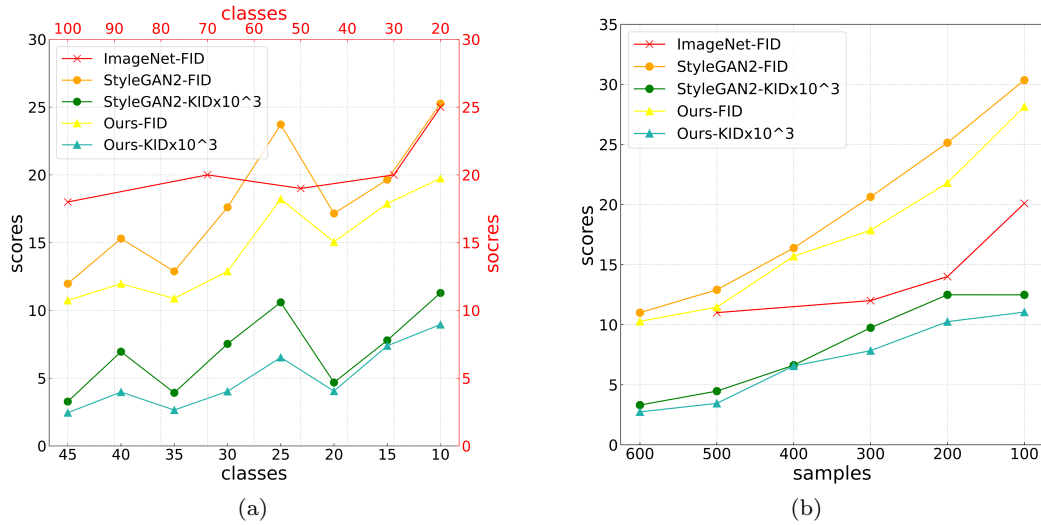


Fig. 2 The FID and KID scores for different experiments on NWPU-RESISC45 dataset training on StyleGAN2+ADA and our method by varying (a) the number of classes and (b) the number of images per class.

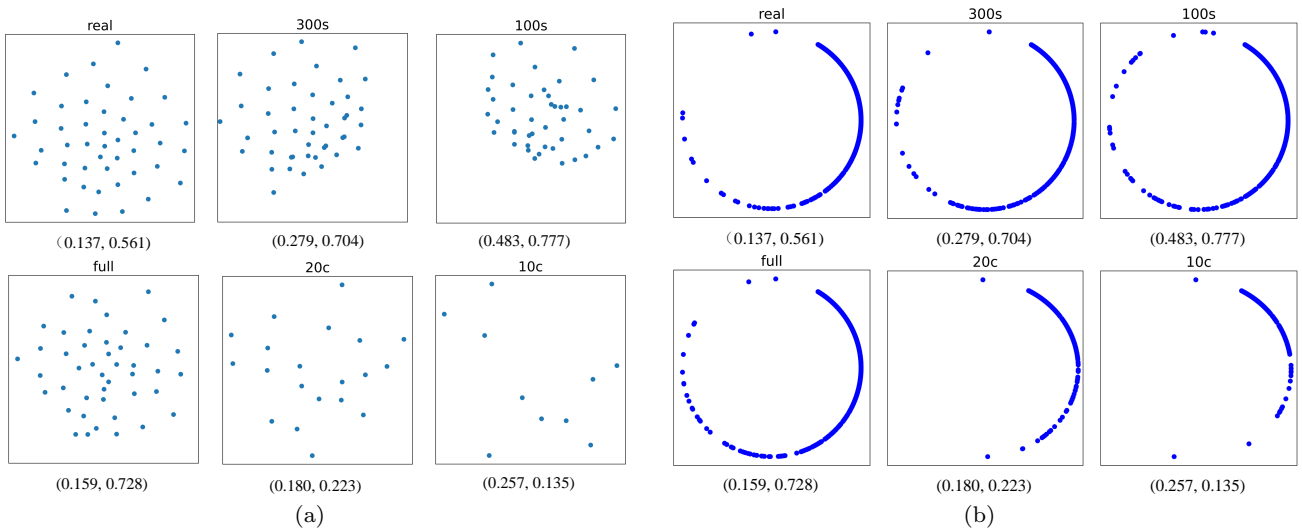


Fig. 3 "real" denotes the features extracted from the real dataset. "full" indicates the features extracted from the samples by the GAN model, which is trained under the original dataset. "c" denotes the number of classes used to train the GAN model, and "s" denotes the number of samples. (a) The distributions of samples in the feature space. The samples are generated by GAN models trained under different data setups. We only show the cluster centers of samples for simplicity. (b) The average feature of samples generated by the same model. The two numbers below each chart are the average pairwise G_2 potential (the lower, the better) of the distributions and the information entropy (the higher, the better) of the features.

3.3 Problem Analysis

For the sensitivity of the GAN model to the size of the RS training dataset, we conjecture that the possible reasons lie in the characteristics of RS images. There are two main differences between RS RGB images and natural images. First, RS images have unique shooting angles. Most RS images are taken from an overhead angle, containing multiple types of objects, such as houses, airplanes and cars. Second, RS images have a larger cov-

erage area. Take the NWPU-RESISC45 dataset as an example. The spatial resolution in this dataset varies from 0.2m to 30m per pixel, while the average scale of a human face is only about 0.2m. Due to these characteristics, RS images usually contain richer feature information than natural images. Thus, for the fluctuations of metrics scores on RS images, the possible reason is that the amount of feature information learned by the GAN model decreases rapidly when the training data decreases.

In order to confirm our conjecture, we analyze the features of the samples generated under different data settings. To this end, we train ResNet-50 on the NWPU-RESISC45 dataset as the feature extraction model and use the output of the last block of ResNet-50 as the features. The StyleGAN2 is trained under different data setups as shown in Fig.2 and generate the same number of samples in each case. We use the pretrained ResNet-50 to extract features from these samples. It is worth to mention that the ResNet-50 is trained under the corresponding number of classes in the case of reducing classes. After obtaining these features, we first conduct dimension reduction and visualize the distribution of these samples in the feature space in Fig.3(a). It can be observed that the distribution of these samples becomes denser as the sample size per class decreases. In contrast, according to the information theory, the uniform distribution has the maximum entropy, indicating richer information. Thus, the feature information learned by the GAN model drops with reduced samples. But it seems that the distributions are affected less in the case of reducing classes. Then we analyze the average feature of samples generated from the same model. In order to show the results more intuitively, every element of the average feature is mapped to a 2-dimensional vector on the unit hypersphere S^1 and visualized in Fig.3(b). As we can see visually from Fig.3(b), the features are affected less when reducing samples, but they get sparser in the case of reducing classes, which means lower information entropy. Thus, the amount of feature information learned by the GAN model also decreases with reduced categories.

From the results of the two experiments above, we can draw a conclusion that the amount of feature information learned by the GAN decreases dramatically as the size of training data reduces. The distribution of samples in the feature space gets denser when reducing samples per class, and the features of individual samples become sparser with reduced classes. Based on this conclusion, we design two novel adjustment schemes that enrich the feature information learned by the GAN model at the distribution and sample levels. As shown in Fig.2, our method, presented next, performs well under various data settings and mitigates the upward trend of the metric curves.

4 Methods

This paper proposes to increase the the amount of feature information contained in the GAN model from two aspects, distribution-wise adjustment and sample-wise adjustment. The overall architecture is shown in Fig.4.

Our methods require neither modification of the network structure nor excessive computational effort and can be used for arbitrary generative models. Next, we will introduce them in detail.

4.1 Distribution-wise Adjustment

In this section, we aim to design distribution-wise adjustment to enrich the feature information learned by the GAN model. According to the definition of information entropy, the greater the entropy is, the more information it contains. It is well known that the uniform distribution has the greatest information entropy. Intuitively, vectors that are roughly uniformly distributed on the unit hypersphere could preserve more information than other vectors. Consequently, we aim to design a novel technique named Uniformity Regularization (UR) over feature space to constrain the feature distribution to a uniform distribution. Designing such a regularization term is in fact nontrivial, it should meet two requirements. To start with, the regularization term should be asymptotically correct, i.e., the distribution optimizing this metric should converge to uniform distribution. Then, the regularization term is supposed to be empirically reasonable with finite number of points. To this end, we consider the Gaussian potential kernel.

$$G(x, y) \triangleq e^{-\gamma\|x-y\|_2^2} = e^{2\gamma x^\top y - 2\gamma}, \quad \gamma > 0 \quad (3)$$

In contrast to other kernels that achieve uniformity of optimal points, the Gaussian kernel is closely related to the universal optimal point configuration and can also be used to represent a general class of other kernels Borodachov et al. (2019). Therefore, the uniformity regularization term is based on Gaussian potential kernel and can be viewed as the logarithm of the average pairwise Gaussian potential, which is shown as follows:

$$\mathcal{L}_{\text{uni}}(f; \gamma) = \log \mathbb{E}_{\substack{\text{i.i.d.} \\ x, y \sim P_G}} \left[e^{-\gamma\|f(x)-f(y)\|_2^2} \right] \quad (4)$$

where P_G denotes the distribution of samples generated by the generator G , f denotes the intermediate layer of generator or discriminator, and $\gamma > 0$ is a hyperparameter.

Theorem 1 *The distribution that minimize the pairwise Gaussian potential is the uniform distribution σ_d on the unit hypersphere S_d .*

Theorem 2 *As number of points reaches infinity, distributions of points minimizing the average pairwise potential converge weak* to the uniform distribution σ_d .*

The proofs of *Theorem 1* and *Theorem 2* can be seen in the Appendix. According to these two theorems, the uniformity regularization term satisfies the

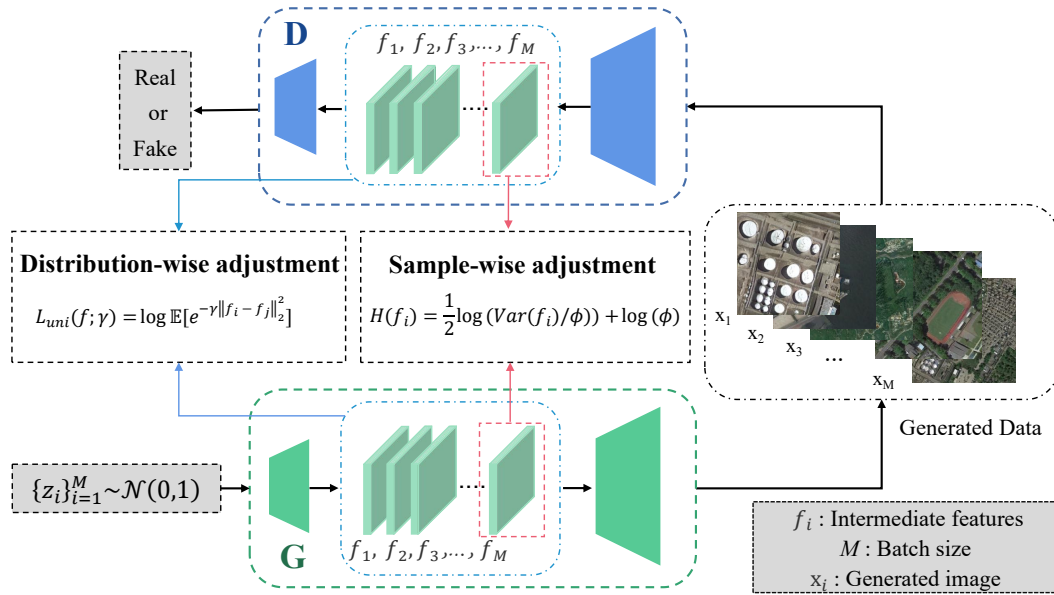


Fig. 4 The overall architecture of our method. G and D are the generator and the discriminator. f denotes the intermediate features. M is the batch size. The real dataset is omitted for clarity as our method is only imposed on generated data.

two requirements above. Besides, we evaluate the average pairwise potential of various finite point collections on S^1 in Fig.3(a). The values are consistent with our intuitive understanding of uniformity.

It has been shown that different network layers are responsible for different levels of detail in the generated image. Empirically, the latter blocks of the generator have more effect on the style (e.g. texture and color) of the image whereas the earlier blocks impact the coarse structure or content of the image Patashnik et al. (2021). Thus, we choose features from a shallow network layer for adjustment in our experiments.

4.2 Sample-wise Adjustment

While previous section focuses on distribution-wise adjustment, this section designs a novel approach at the sample level to increase the amount of feature information learned by the GAN model. Inspired by the principle of maximum entropy in information theory, we propose sample-wise adjustment to increase the entropy of the features from a single generated sample. To this end, we design an Entropy Regularization (ER) term to calculate entropy of the intermediate features $f(x)$.

Since the feature distribution is a high dimensional function, it is difficult to compute the precise value of its entropy directly. Fortunately, based on the *Theorem 3* Thomas and Joy (2006), we could estimate the upper bound of the entropy.

Theorem 3 For any continuous distribution $P(x)$ of mean μ and variance σ^2 , its differential entropy is maximized when $P(x)$ is a Gaussian distribution $N(\mu, \sigma^2)$.

According to *Theorem 3*, the entropy of a distribution is upper bounded by a Gaussian distribution with the same mean and variance. The entropy of a Gaussian distribution is shown in Eq.5:

$$H^*(x) = \frac{1}{2} \log(2\pi) + \frac{1}{2} + H(x) \quad (5)$$

$$H(x) := \log(\sigma)$$

where x is sampled from the Gaussian distribution $N(\mu, \sigma^2)$.

Since the entropy of Gaussian distribution only depends on the variance, we could use $H(x)$ instead of $H^*(x)$. Based on these discussions, the upper bound entropy of the intermediate features $f(x)$ is shown in Eq.6:

$$H(f(x)) = \frac{1}{2} \log(\text{Var}(f(x))) \quad (6)$$

where x is a generated image.

To avoid numerical overflow, we re-scale features $f(x)$ by a constant ϕ , and then compensate the entropy of the features by multiplying this constant. In our experiments, we set ϕ to the L2 norm of the features. We evaluate the entropy of the features in Fig.3(b). The results prove the efficacy of our method. In addition, same as previous section, we choose features from a shallow network layer for adjustment.

$$H(f(x)) = \frac{1}{2} \log(\text{Var}(f(x)/\phi)) + \log(\phi) \quad (7)$$

4.3 Overall Objective

The final loss function of the generator is shown in Eq.8:

$$L_G = L_{\text{ori}} + \lambda_G L_{\text{uni}}^G + \lambda_D L_{\text{uni}}^D - \delta_G \sum H^G - \delta_D \sum H^D \quad (8)$$

where L_{ori} represents the original loss function of generator. L_{uni}^G and L_{uni}^D denote the uniformity regularization on features from the generator and the discriminator respectively. H^G and H^D denote the entropy regularization on features from the generator and the discriminator respectively. λ_G , λ_D , δ_G , and δ_D are hyperparameters.

5 Experiment

In this section, we first provide the details of our experimental setup. Then, we present the quantitative and qualitative results of the proposed method, as well as the comparison with existing methods. Finally, we provide more ablation and analysis of different components of our method. In our experiments, "real" denotes real data. "full" indicates the original dataset. "c" denotes the number of classes used to train the GAN model, and "s" denotes the number of samples.

5.1 Experiment Setup

Datasets: We use two remote sensing datasets to evaluate our method: NWPU-RESISC45 Dataset and PatternNet Dataset. To evaluate our methods under different data set up, we decrease the number of classes and images per class in these datasets using random sampling.

The NWPU-RESISC45 Dataset [Gong et al. \(2017\)](#) has 31,500 images covering more than 100 countries and regions around the world. It has 45 categories with 700 images in each category. Each image is 256×256 pixels in size. The spatial resolution of this dataset is up to 0.2m and the lowest is 30m. In addition, the images are varied in lighting, shooting angle, imaging conditions, and so on.

The PatternNet Dataset [Zhou et al. \(2018\)](#) is a large-scale high-resolution remote sensing dataset. It has 38 categories with 800 images in each category. Each image is 256×256 pixels in size. The spatial resolution of this dataset varies from 0.06m per pixel to 4.7m per pixel. The images in PatternNet are collected from Google Earth imagery or via the Google Map API for some US cities.

Implementation details: We base our method on two different models **StyleGAN2** [Karras et al. \(2020b\)](#)

and **BigGAN** [Brock et al. \(2018\)](#) with different augmentation methods **ADA** [Karras et al. \(2020a\)](#) and **APA** [Jiang et al. \(2021a\)](#), and regularization method **LeCam** [Tseng et al. \(2021\)](#). We use the official PyTorch implementation of StyleGAN2+ADA. For StyleGAN2+APA, BigGAN and LeCam, we use the implementations provided by [Kang and Park \(2020\)](#).

Evaluation Metrics: We evaluate our method using Frechet inception distance (FID) [Heusel et al. \(2017\)](#), as the most commonly-used metric for measuring the quality and diversity of images generated by GAN models. We also include Kernel Inception Distance (KID) [Bińkowski et al. \(2018\)](#) as a metric that is unbiased by empirical bias [Xu et al. \(2018a\)](#).

5.2 Results and Comparisons

We first visualize the distributions and features of our method in Fig.5. Compared with Fig.3, the distributions of generated images in the feature space under fewer training samples become more uniform (Fig.5(a)), and the features of the individual images under fewer training classes are denser (Fig.5(b)). The experiment results prove the efficacy of our methods. Then, we provide a quantitative comparison with the well-established baselines. Results are reported in Table 1. The red numbers indicate the improvement of the GAN models after using our method. In general, the FID and KID scores for our proposed method indicate a significant and consistent advantage over all the compared methods. In detail, our comparison experiments can be divided into three types. First, under different model structures, BigGAN and StyleGAN2, our method is robust, which proves that our approach can be applied to any model architecture. Second, under different augmentation methods, ADA and APA. The results of ADA are better than those of APA on RS datasets. Nevertheless, our method still performs well. This shows that the proposed regularization approaches can be applied to other GAN models along with existing augmentation approaches. Third, combined with the regularization method LeCam, our method is still effective. The proposed method can be viewed as an effective complement to existing regularization methods. The generated images and FID curves of StyleGAN2 and BigGAN with different optimized approaches during training are visualized in the Appendix. These experiment results prove the effectiveness and versatility of our methods.

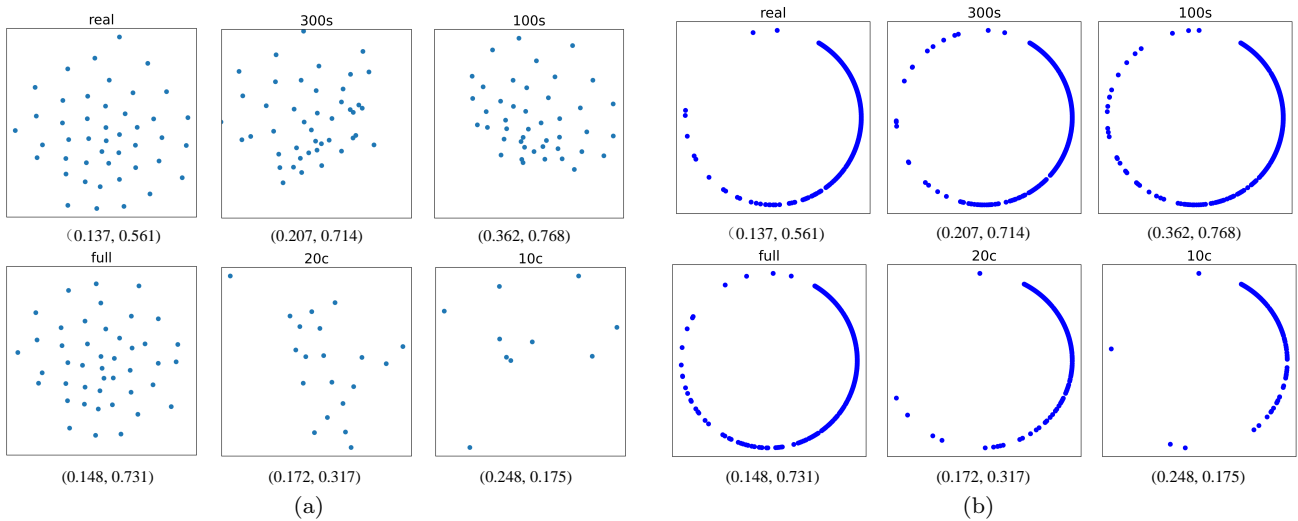


Fig. 5 (a) The distributions of samples generated by our methods in the feature space. (b) The average feature of samples generated by the same model. The two numbers below each chart are the average pairwise G_2 potential (the lower, the better) and the information entropy (the higher, the better).

Table 1 Comparison of Quality Scores on the NWPU-RESISC45 and PatternNet Dataset (the red numbers present our improvement)

Methods	NWPU-RESISC45		PatternNet	
	FID↓	KID↓	FID↓	KID↓
BigGAN+ADA	30.91- 2.09	10.13- 1.41	43.94- 1.59	16.71- 1.03
BigGAN+ADA+LeCam	32.65- 2.24	11.69- 1.65	41.28- 3.42	15.89- 1.97
StyleGAN2+APA	21.67- 2.91	8.54- 1.90	33.75- 1.84	12.34- 2.33
StyleGAN2+ADA	11.97- 1.23	3.27- 0.82	33.53- 2.06	12.67- 1.92
StyleGAN2+ADA+LeCam	14.38- 2.68	4.97- 1.39	31.32- 2.11	11.32- 0.89

Table 2 Ablation study on the regularization components

Methods	NWPU			PN		
	full	300s	15c	full	300s	18c
Baseline	11.97	20.63	19.64	33.53	44.21	28.88
Only UR	11.28	17.86	18.26	31.48	42.03	27.67
Only ER	11.20	18.24	18.04	32.87	43.25	26.61
Ours	10.74	16.89	17.88	32.55	41.73	25.22

5.3 Ablation and Analysis

In this section, we provide further ablation and analysis over different components of our method.

Regularization components. We provide an ablation study containing four different variants. Table 2 presents the results of the ablation study on NWPU-RESISC45 and PatternNet datasets. The No Regularization version yields poor results as expected. Adding the uniformity regularization already brings significant

Table 3 Ablation study on temperature parameter γ

γ	2	3	5	7
FID	15.05	16.70	17.85	24.96

improvement to the model under different data setups. The entropy regularization is also effective in most cases. As proposed in our final method, adding both uniformity and entropy regularization in the loss function of the generator achieves the best results. The detailed ablation study under different data settings is presented in the Appendix.

Temperature parameter and other hyperparameters. First, we conduct the ablation study on temperature parameter γ using StyleGAN2+ADA on NWPU-RESISC45 dataset with twenty classes. The FID scores are shown in Table 3. Based on the experiment results, we set $\gamma = 2$ in the following experiments.

Table 4 Ablation study on hyperparameters λ_G and λ_D

(λ_G, λ_D)	NWPU			PN		
	full	300s	15c	full	300s	18c
(0, 0.2)	11.24	19.76	18.33	33.70	42.48	27.39
(0.2, 0)	14.78	20.98	19.27	34.63	43.5	29.24
(0.2, 0.2)	11.96	17.24	18.09	31.48	41.73	25.22
(0.5, 0.5)	10.74	16.89	17.88	33.24	41.39	27.01

Table 5 Ablation study on hyperparameters δ_G and δ_D

(δ_G, δ_D)	NWPU			PN		
	full	300s	15c	full	300s	18c
(0, 0.1)	12.08	18.21	19.03	33.15	42.18	27.41
(0.1, 0)	13.62	21.14	19.79	35.63	45.09	28.56
(0.1, 0.1)	10.74	16.89	17.88	33.21	42.53	26.44
(0.2, 0.2)	11.29	17.32	18.46	31.48	41.39	25.22

Table 6 Ablation study on features from different blocks

Block	4	6	8	10	12
FID	17.26	15.92	15.05	20.23	32.19

Then we conduct sensitive studies on hyperparameters using StyleGAN2+ADA on NWPU-RESISC45 and PatternNet dataset. Part of the results is shown in Table 4 and Table 5. The model gets better results when using features from both the generator and the discriminator, which is our final loss function. Detailed results of the ablation experiments on these hyperparameters are in the Appendix. We set $\lambda_G = 0.5$, $\lambda_D = 0.5$, $\delta_G = 0.1$, and $\delta_D = 0.1$ for NWPU-RESISC45 dataset, $\lambda_G = 0.2$, $\lambda_D = 0.3$, $\delta_G = 0.2$, and $\delta_D = 0.2$ for PatternNet dataset in our experiments.

Feature selection. Next, we conduct ablation studies on features from different network layers. As we mentioned before, different network layers are related to different levels of details in the generated image, and the earlier blocks of the network impact the coarse structure or content of the image. We conduct experiments on StyleGAN2+ADA model, which consists of 14 blocks. We choose 5 blocks for comparison, and the results are shown in Table 6. We empirically choose the outputs of 8th block as the features in our method, which is also in line with our previous analysis (Section 4.1).

6 Conclusion

In this work, we first explore the properties of GAN models on RS images and find that the GAN model

is more sensitive to the training data size for RS image generation than for natural image generation. With fewer classes or samples per class, the distribution of generated samples in the feature space becomes clustered, and the features of individual samples get sparser, indicating lower information entropy. Based on this discovery, we conclude that the amount of feature information learned by the GAN decreases dramatically as the training dataset reduces, leading to poor generation quality. Then, we design distribution-wise and sample-wise regularization schemes to increase the information entropy and enrich the feature information contained in the GAN model. We theoretically and empirically prove the effectiveness of our methods. Extensive experiments on two RS datasets show the advantages and versatility of our methods.

Acknowledgements The authors would like to acknowledge the support and the collaboration effort of the project team. This work was supported by National Natural Science Foundation of China (91938301).

Conflict of interest

The authors declare that they have no conflict of interest.

References

- Abady L, Barni M, Garzelli A, Tondi B (2020) Gan generation of synthetic multispectral satellite images. In: Image and Signal Processing for Remote Sensing XXVI, SPIE, vol 11533, pp 122–133
- Arjovsky M, Chintala S, Bottou L (2017) Wasserstein GAN. arXiv e-prints arXiv:1701.07875, [1701.07875](#)
- Bejiga MB, Hoxha G, Melgani F (2020) Improving text encoding for retro-remote sensing. IEEE Geoscience and Remote Sensing Letters 18(4):622–626
- Bell-Kligler S, Shocher A, Irani M (2019) Blind super-resolution kernel estimation using an internal-gan. Advances in Neural Information Processing Systems 32
- Bińkowski M, Sutherland DJ, Arbel M, Gretton A (2018) Demystifying mmd gans. In: International Conference on Learning Representations
- Borodachov SV, Hardin DP, Saff EB (2019) Discrete energy on rectifiable sets. Springer
- Brock A, Donahue J, Simonyan K (2018) Large scale gan training for high fidelity natural image synthesis. In: International Conference on Learning Representations

- Chen H, Li W, Shi Z (2021) Adversarial instance augmentation for building change detection in remote sensing images. *IEEE Transactions on Geoscience and Remote Sensing* 60:1–16
- Chen X, Chen S, Xu T, Yin B, Peng J, Mei X, Li H (2020) Smapgan: Generative adversarial network-based semisupervised styled map tile generation method. *IEEE Transactions on Geoscience and Remote Sensing* 59(5):4388–4406
- Choi J, Kim T, Kim C (2019) Self-ensembling with gan-based data augmentation for domain adaptation in semantic segmentation. In: *Proceedings of the IEEE/CVF International Conference on Computer Vision*, pp 6830–6840
- Esser P, Rombach R, Ommer B (2021) Taming transformers for high-resolution image synthesis. In: *Proceedings of the IEEE/CVF conference on computer vision and pattern recognition*, pp 12873–12883
- Gao F, Liu Q, Sun J, Hussain A, Zhou H (2019) Integrated gans: Semi-supervised sar target recognition. *IEEE Access* 7:113999–114013
- Gong C, Han J, Lu X (2017) Remote sensing image scene classification: Benchmark and state of the art. *Proceedings of the IEEE* 105(10):1865–1883
- Goodfellow IJ, Pouget-Abadie J, Mirza M, Xu B, Warde-Farley D, Ozair S, Courville A, Bengio Y (2014) Generative adversarial nets. In: *Proceedings of the 27th International Conference on Neural Information Processing Systems - Volume 2*, MIT Press, Cambridge, MA, USA, NIPS'14, p 2672–2680
- Gulrajani I, Ahmed F, Arjovsky M, Dumoulin V, Courville AC (2017) Improved training of wasserstein gans. *Advances in neural information processing systems* 30
- Gulrajani I, Raffer C, Metz L (2018) Towards gan benchmarks which require generalization. In: *International Conference on Learning Representations*
- He J, Shi W, Chen K, Fu L, Dong C (2022) Gcfsr: a generative and controllable face super resolution method without facial and gan priors. In: *Proceedings of the IEEE/CVF Conference on Computer Vision and Pattern Recognition*, pp 1889–1898
- Heusel M, Ramsauer H, Unterthiner T, Nessler B, Hochreiter S (2017) Gans trained by a two time-scale update rule converge to a local nash equilibrium. *Advances in neural information processing systems* 30
- Hinton GE, Salakhutdinov RR (2006) Reducing the dimensionality of data with neural networks. *science* 313(5786):504–507
- Jiang K, Wang Z, Yi P, Wang G, Lu T, Jiang J (2019) Edge-enhanced gan for remote sensing image super-resolution. *IEEE Transactions on Geoscience and Remote Sensing* 57(8):5799–5812
- Jiang L, Dai B, Wu W, Loy CC (2021a) Deceive d: Adaptive pseudo augmentation for gan training with limited data. *Advances in Neural Information Processing Systems* 34:21655–21667
- Jiang Y, Chang S, Wang Z (2021b) Transgan: Two pure transformers can make one strong gan, and that can scale up. *Advances in Neural Information Processing Systems* 34:14745–14758
- Jolicœur-Martineau A (2018) The relativistic discriminator: a key element missing from standard gan. *arXiv preprint arXiv:180700734*
- Kang M, Park J (2020) Contragan: Contrastive learning for conditional image generation. *Advances in Neural Information Processing Systems* 33:21357–21369
- Karras T, Laine S, Aila T (2019) A style-based generator architecture for generative adversarial networks. In: *Proceedings of the IEEE/CVF conference on computer vision and pattern recognition*, pp 4401–4410
- Karras T, Aittala M, Hellsten J, Laine S, Lehtinen J, Aila T (2020a) Training generative adversarial networks with limited data. *Advances in Neural Information Processing Systems* 33:12104–12114
- Karras T, Laine S, Aittala M, Hellsten J, Lehtinen J, Aila T (2020b) Analyzing and improving the image quality of stylegan. In: *Proceedings of the IEEE/CVF conference on computer vision and pattern recognition*, pp 8110–8119
- Ledig C, Theis L, Huszár F, Caballero J, Cunningham A, Acosta A, Aitken A, Tejani A, Totz J, Wang Z, et al. (2017) Photo-realistic single image super-resolution using a generative adversarial network. In: *Proceedings of the IEEE conference on computer vision and pattern recognition*, pp 4681–4690
- Li L, Li P, Yang M, Gao S (2019) Multi-branch semantic gan for infrared image generation from optical image. In: Cui Z, Pan J, Zhang S, Xiao L, Yang J (eds) *Intelligence Science and Big Data Engineering. Visual Data Engineering*, Springer International Publishing, Cham, pp 484–494
- Lin D, Fu K, Wang Y, Xu G, Sun X (2017) Marta gans: Unsupervised representation learning for remote sensing image classification. *IEEE Geoscience and Remote Sensing Letters* 14(11):2092–2096, DOI 10.1109/LGRS.2017.2752750
- Liu B, Zhu Y, Song K, Elgammal A (2020) Towards faster and stabilized gan training for high-fidelity few-shot image synthesis. In: *International Conference on Learning Representations*
- Liu MY, Tuzel O (2016) Coupled generative adversarial networks. *Advances in neural information processing systems* 29
- Mao X, Li Q, Xie H, Lau RY, Wang Z, Paul Smolley S (2017) Least squares generative adversarial networks.

- In: Proceedings of the IEEE international conference on computer vision, pp 2794–2802
- Mescheder L, Geiger A, Nowozin S (2018) Which training methods for gans do actually converge? In: International conference on machine learning, PMLR, pp 3481–3490
- Miyato T, Kataoka T, Koyama M, Yoshida Y (2018) Spectral Normalization for Generative Adversarial Networks. arXiv e-prints arXiv:1802.05957, [1802.05957](#)
- Park T, Liu MY, Wang TC, Zhu JY (2019) Semantic image synthesis with spatially-adaptive normalization. In: Proceedings of the IEEE/CVF conference on computer vision and pattern recognition, pp 2337–2346
- Patashnik O, Wu Z, Shechtman E, Cohen-Or D, Lischinski D (2021) Styleclip: Text-driven manipulation of stylegan imagery. In: Proceedings of the IEEE/CVF International Conference on Computer Vision, pp 2085–2094
- Ranzato M, Mnih V, Hinton GE (2010) Generating more realistic images using gated mrf's. Advances in Neural Information Processing Systems 23
- Rui X, Cao Y, Yuan X, Kang Y, Song W (2021) Disastergan: Generative adversarial networks for remote sensing disaster image generation. Remote Sensing 13(21), DOI 10.3390/rs13214284
- Shahbazi M, Danelljan M, Paudel DP, Gool LV (2022) Collapse by conditioning: Training class-conditional GANs with limited data. In: International Conference on Learning Representations
- Su X, Lin Y, Zheng Q, Wu F, Zheng C, Zhao J (2022) Gsgan: Learning controllable geospatial images generation. IET Image Processing
- Thomas M, Joy AT (2006) Elements of information theory. Wiley-Interscience
- Tseng HY, Jiang L, Liu C, Yang MH, Yang W (2021) Regularizing generative adversarial networks under limited data. In: Proceedings of the IEEE/CVF Conference on Computer Vision and Pattern Recognition, pp 7921–7931
- Wang SY, Bau D, Zhu JY (2021) Sketch your own gan. In: Proceedings of the IEEE/CVF International Conference on Computer Vision, pp 14050–14060
- Webster R, Rabin J, Simon L, Jurie F (2019) Detecting overfitting of deep generative networks via latent recovery. In: Proceedings of the IEEE/CVF Conference on Computer Vision and Pattern Recognition, pp 11273–11282
- Wei Y, Luo X, Hu L, Peng Y, Feng J (2020) An improved unsupervised representation learning generative adversarial network for remote sensing image scene classification. Remote Sensing Letters 11(6):598–607
- Xiong Y, Guo S, Chen J, Deng X, Sun L, Zheng X, Xu W (2020) Improved srgan for remote sensing image super-resolution across locations and sensors. Remote Sensing 12(8):1263
- Xu L, Jordan MI (1996) On convergence properties of the em algorithm for gaussian mixtures. Neural computation 8(1):129–151
- Xu Q, Huang G, Yuan Y, Guo C, Sun Y, Wu F, Weinberger KQ (2018a) An empirical study on evaluation metrics of generative adversarial networks. arXiv preprint arXiv:180607755
- Xu Y, Du B, Zhang L (2018b) Can we generate good samples for hyperspectral classification?—a generative adversarial network based method. In: IGARSS 2018-2018 IEEE International Geoscience and Remote Sensing Symposium, IEEE, pp 5752–5755
- Yu J, Lin Z, Yang J, Shen X, Lu X, Huang TS (2018) Generative image inpainting with contextual attention. In: Proceedings of the IEEE conference on computer vision and pattern recognition, pp 5505–5514
- Yu Y, Li X, Liu F (2019) Attention gans: Unsupervised deep feature learning for aerial scene classification. IEEE Transactions on Geoscience and Remote Sensing 58(1):519–531
- Zeng Y, Lin Z, Lu H, Patel VM (2021) Cr-fill: Generative image inpainting with auxiliary contextual reconstruction. In: Proceedings of the IEEE/CVF International Conference on Computer Vision, pp 14164–14173
- Zhang H, Goodfellow I, Metaxas D, Odena A (2019) Self-attention generative adversarial networks. In: International conference on machine learning, PMLR, pp 7354–7363
- Zhao B, Zhang S, Xu C, Sun Y, Deng C (2021) Deep fake geography? when geospatial data encounter artificial intelligence. Cartography and Geographic Information Science 48(4):338–352
- Zhao S, Liu Z, Lin J, Zhu JY, Han S (2020) Differentiable augmentation for data-efficient gan training. Advances in Neural Information Processing Systems 33:7559–7570
- Zhou W, Newsam S, Li C, Shao Z (2018) Patternnet: A benchmark dataset for performance evaluation of remote sensing image retrieval. ISPRS journal of photogrammetry and remote sensing 145:197–209